Supporting Information

One Step Phenol Synthesis from Benzene Catalysed by Nickel(II) Complexes

Sethuraman Muthuramalingam,[a] Karunanithi Anandababu,[a] Marappan Velusamy,[b] and Ramasamy Mayilmurugan*,[a]

[a]Bioinorganic Chemistry Laboratory/Physical Chemistry, School of Chemistry, Madurai Kamaraj University, Madurai 625021, India. Email: mayilmurugan.chem@mkuniversity.org

[b]Department of Chemistry, North Eastern Hill University, Shillong 793022, India.

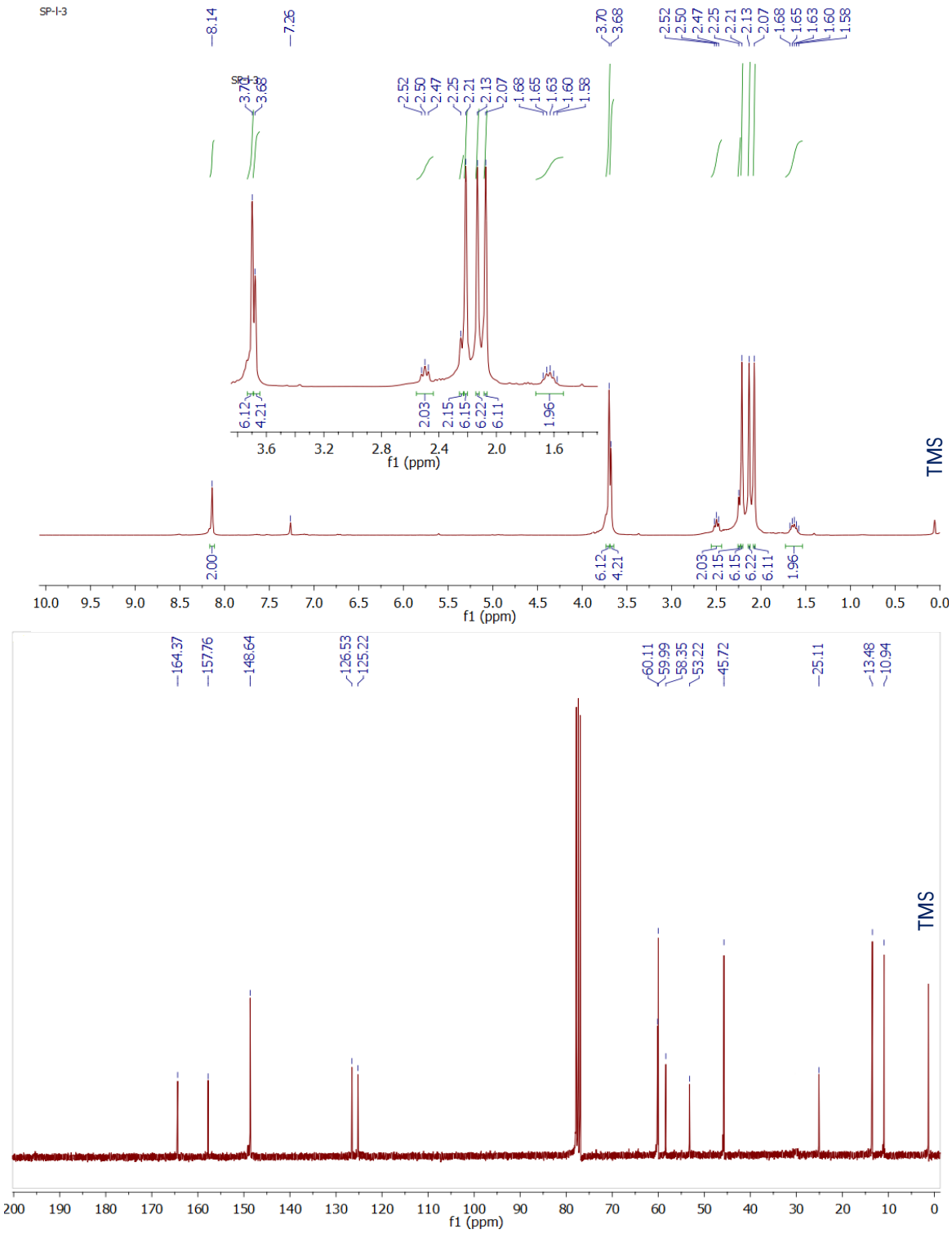

Figure S1. ^{1}H and ^{13}C NMR spectra for L3 in $CDCl_3$.

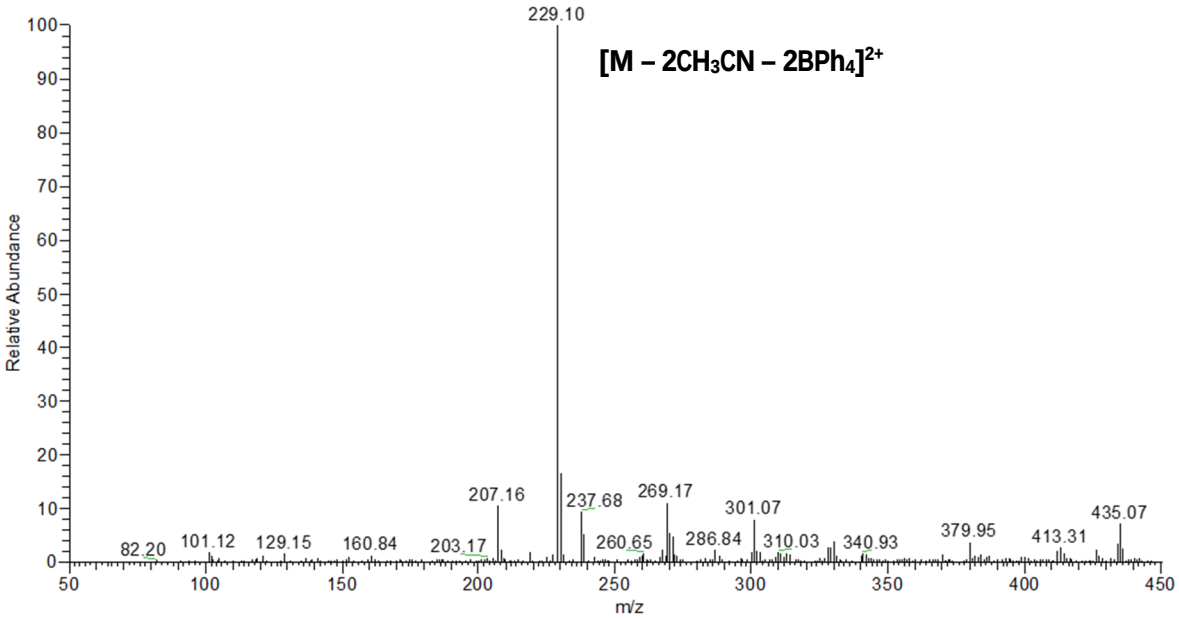

Figure S2. ESI-Mass spectra of **3** in acetonitrile.

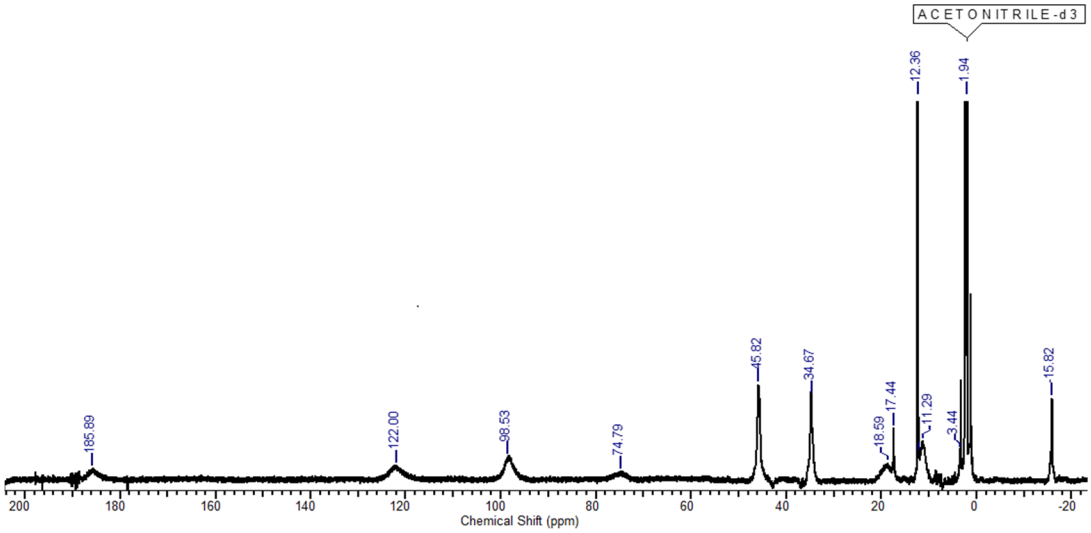

Figure S3. Paramagnetic ^{1}H NMR spectra for **4** in CD_3CN.

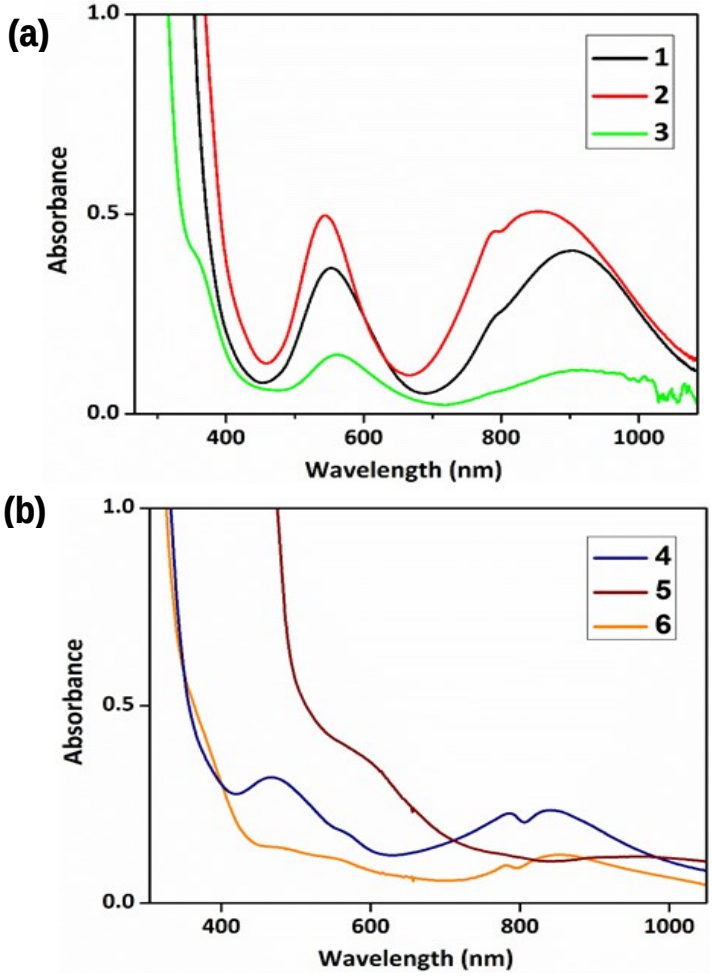

Figure S4. Electronic spectra of **1 - 3 (a)** and **4 - 6 (b)** (5×10^{-3} M) in acetonitrile at 25 °C.

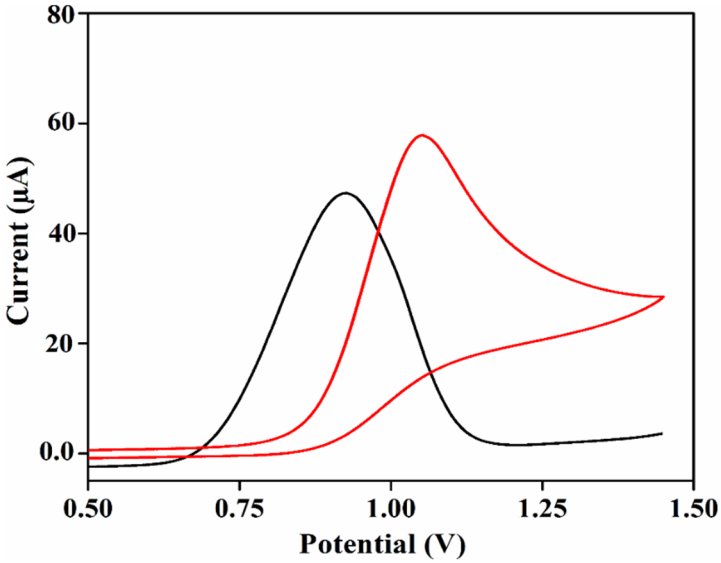

Figure S5. Cyclic voltammogram and differential pulse voltammogram of **3** (5×10^{-3} M) in acetonitrile at 25 °C. Supporting electrolyte: 0.5 M TBAP; Reference: Ag/Ag^{+}; working electrode: Pt-sphere; Counter electrode: Pt wire.

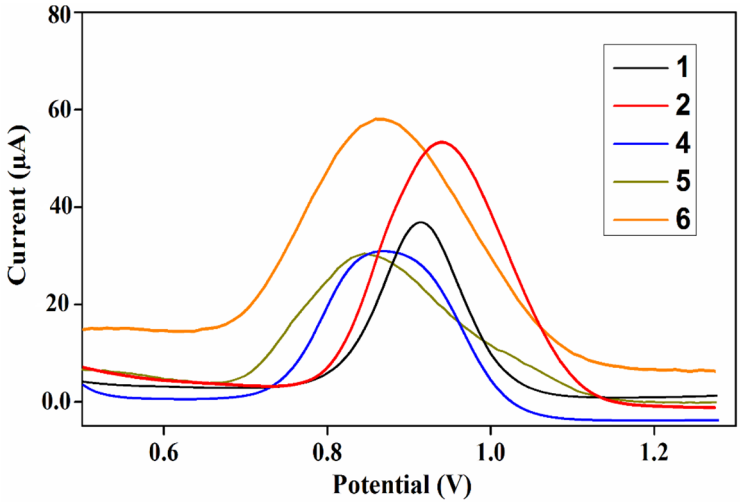

Figure S6. Differential pulse voltammogram of **1 - 2** and **4 - 6** (5×10^{-3} M) in acetonitrile at 25 °C. Supporting electrolyte: 0.5 M TBAP; Reference: Ag/Ag^{+}; working electrode: Pt-sphere; Counter electrode: Pt wire.

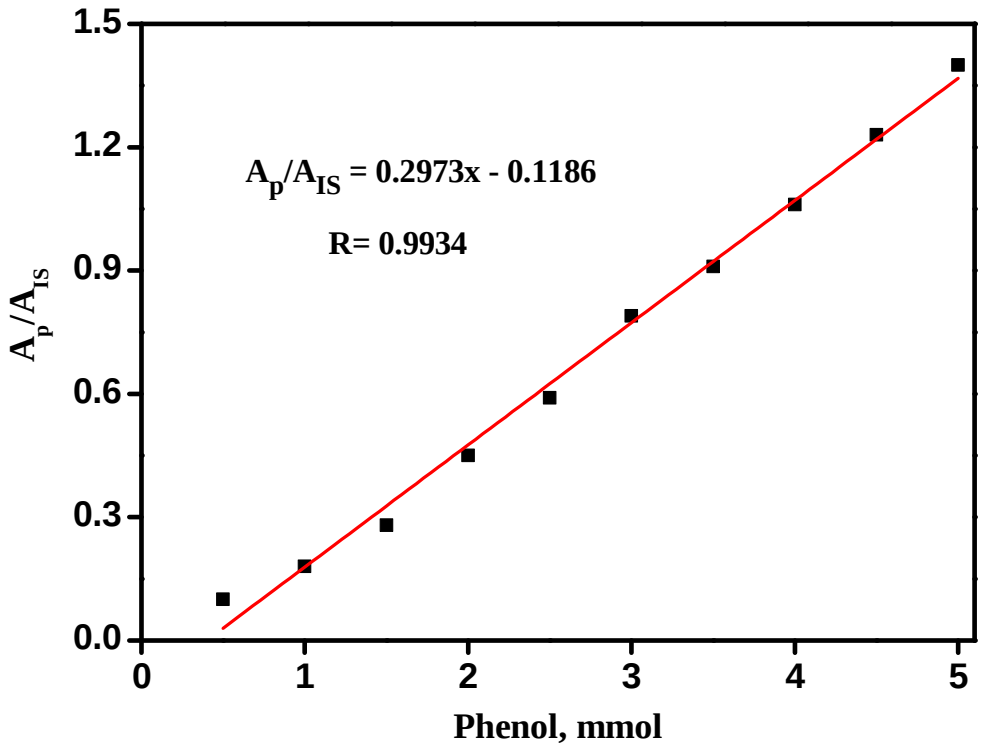

Figure S7. The standard calibration curve using GC, area ratio of phenol to the internal standard (nitrobenzene) (A_P/A_{IS})[a]. [a]A is designated as the chromatographic peak area; p stands for phenol and IS stands for internal standard (nitrobenzene).

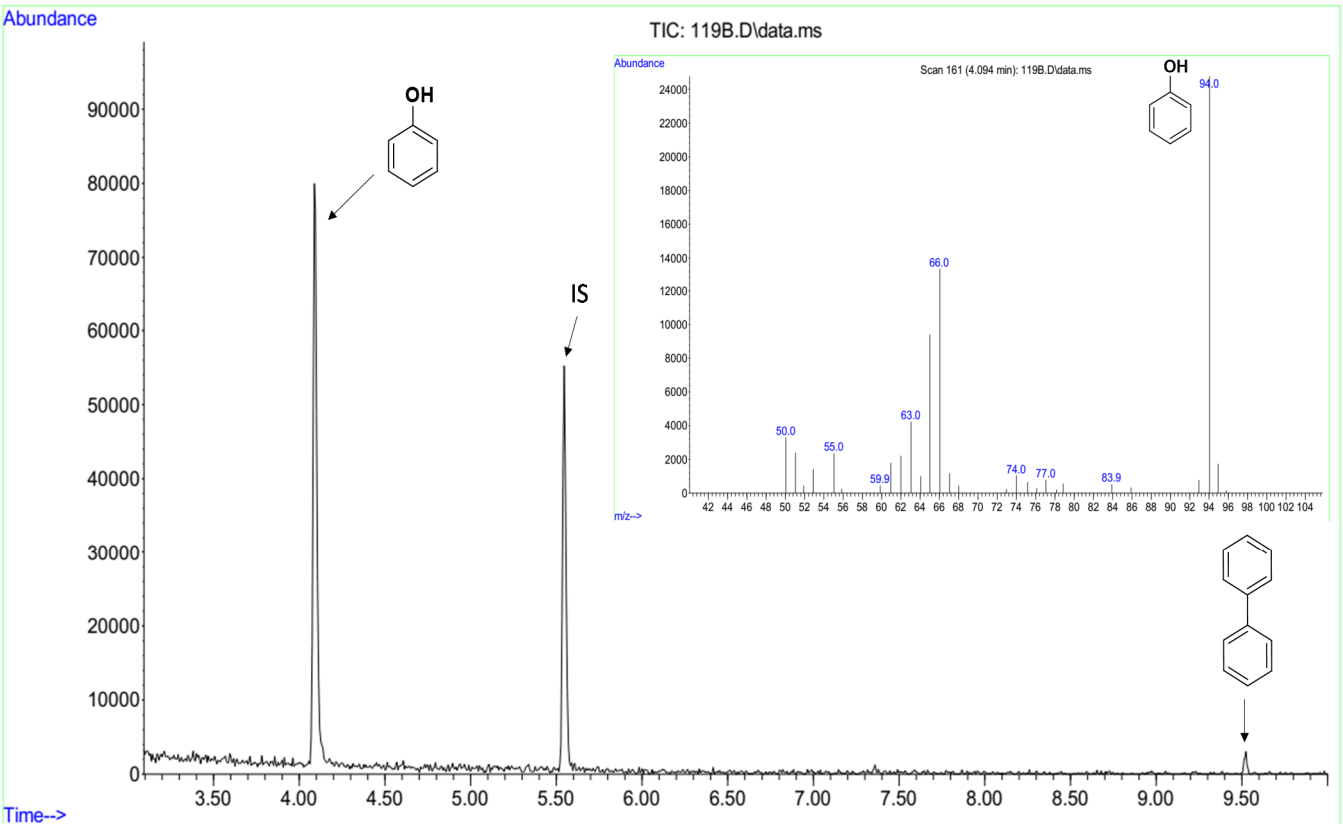

Figure S8. GC-MS profile for the formation of phenol using catalyst **3** and in presence of nitrobenzene as an internal standard.

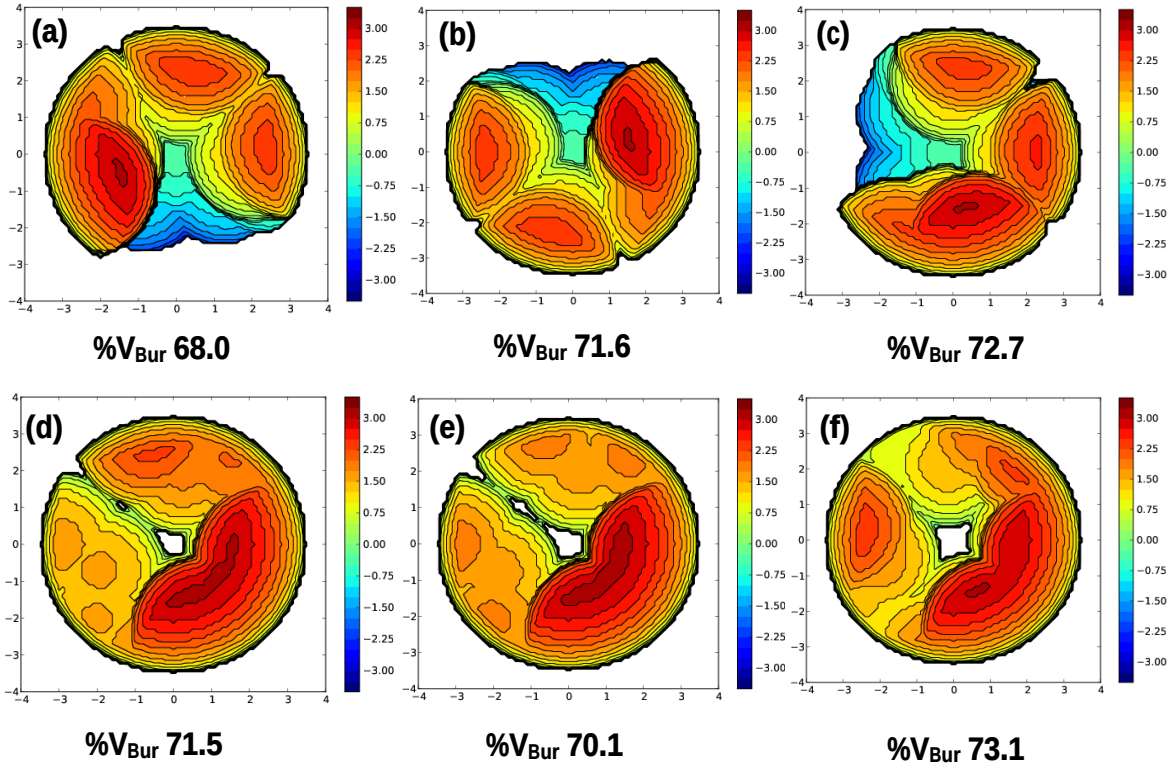

Figure S9. Steric map of complex **1 (a), 2 (b), 3 (c), 4 (d), 5 (e)** and **6 (f)**.

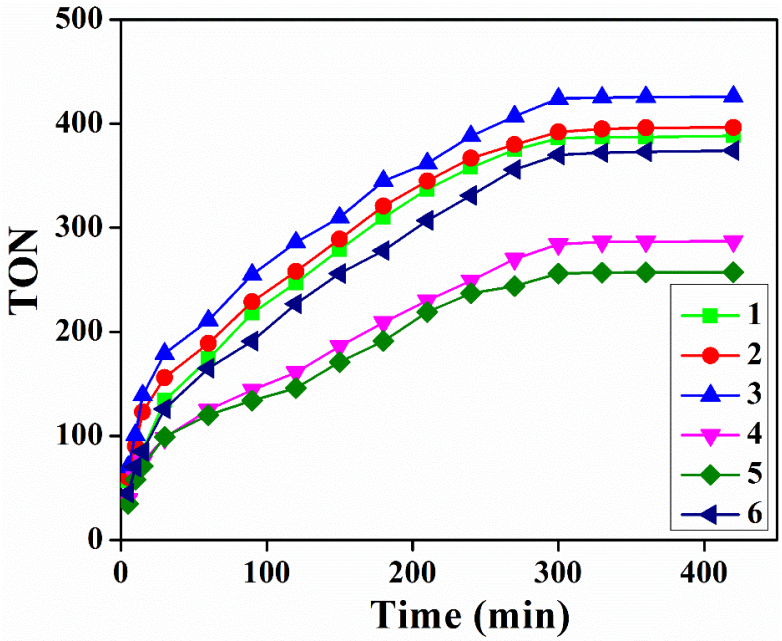

Figure S10. Time courses of the phenol formation from benzene (5 mmol) with H_2O_2 (25 mmol) in the presence of **1 – 6** (2.5 μmol) and Et_3N (5 μmol) in acetonitrile (3.0 mL) at 25°C.

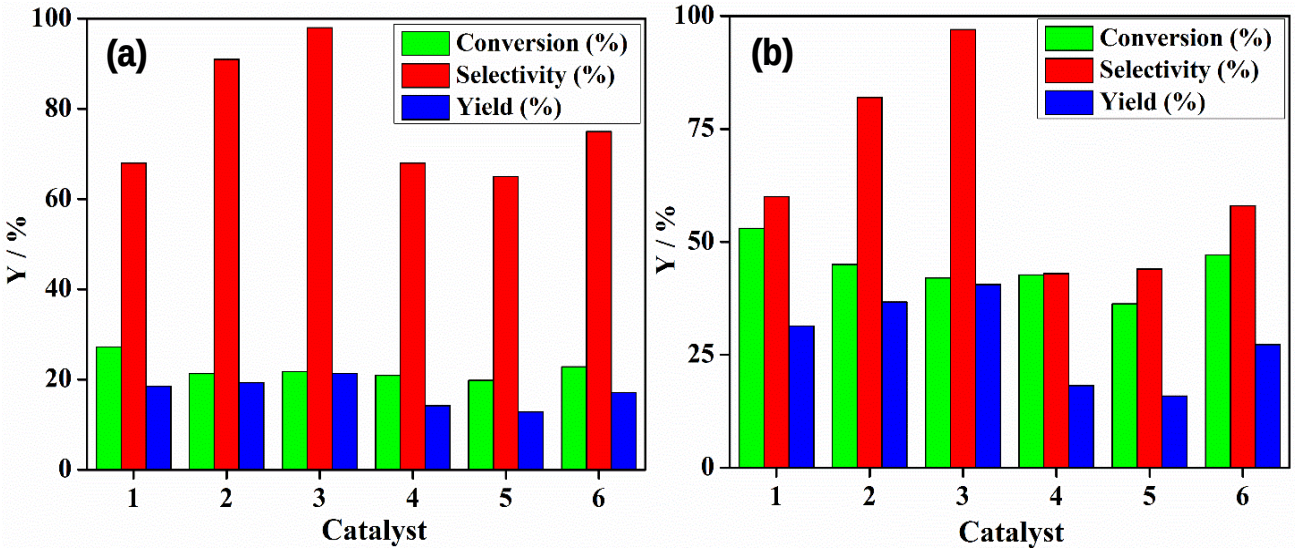

Figure S11. Plot of phenol conversion, selectivity, and yield from benzene (5 mmol) catalyzed by **1 - 6** (2.5 μmol) in the presence of aqueous H_2O_2 (25 mmol) and Et_3N (5 μmol) at 25°C (**a**) and 60 °C **(b).**

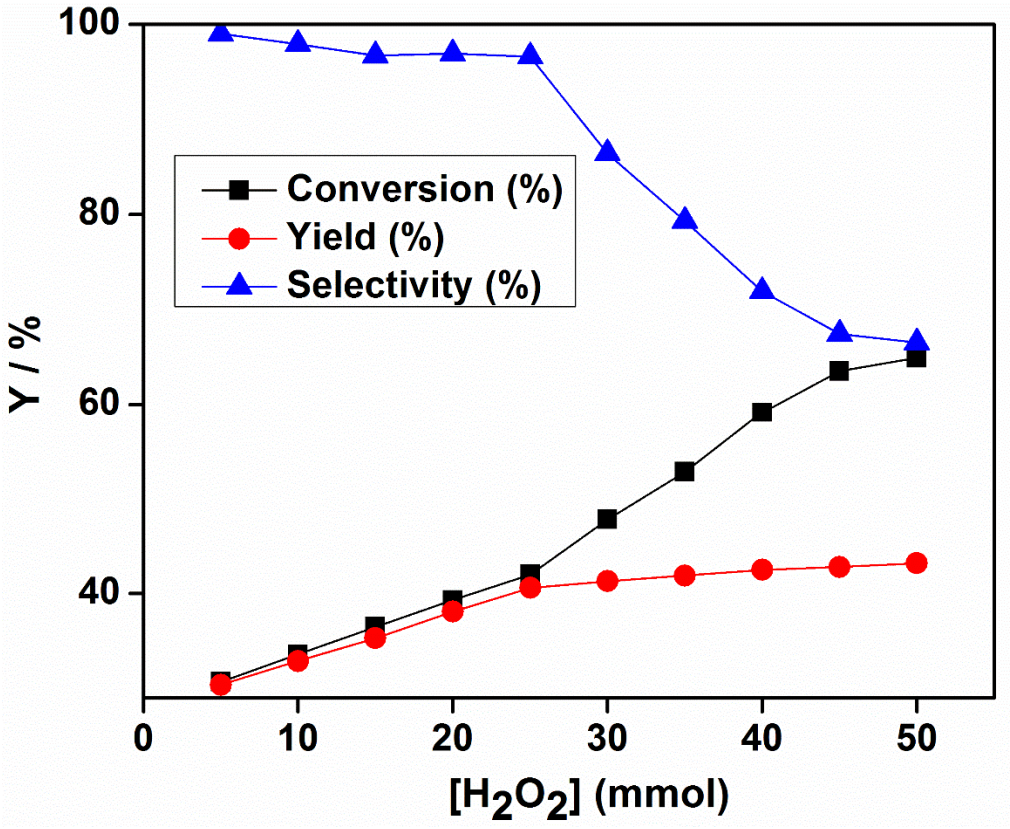

Figure S12. H_2O_2 dependent catalytic hydroxylation of benzene (5 mmol) catalyzed by **3** (2.5 μmol) and Et_3N (5 μmol) in acetonitrile (3.0 mL) at 60 °C.

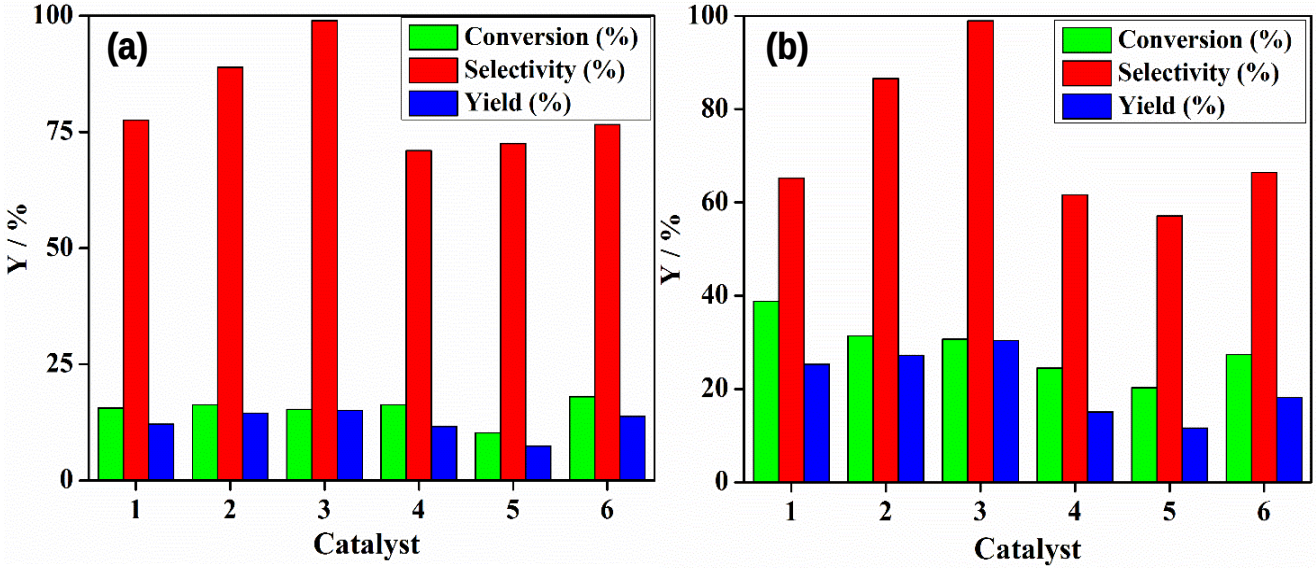

Figure S13. Plot of conversion, selectivity, and yield from benzene (5 mmol) catalyzed by **1 - 6** (2.5 μmol) in the presence of aqueous H_2O_2 (5 mmol) and Et_3N (5 μmol) at 25°C (**a**) and 60 °C (**b**).

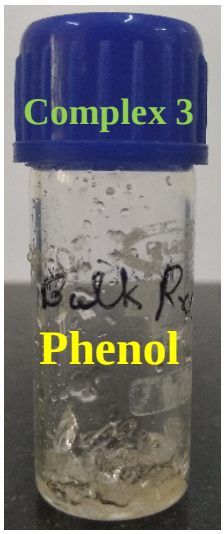

Figure S14. Bulk scale phenol production using catalyst **3**. Reaction condition: benzene (30 mmol, 2.7 mL), **3** (0.05 mmol, 0.043 g), Et_3N (0.1 mmol), 30% aqueous H_2O_2 (100 mmol) in CH_3CN (20 mL) at 60 °C for 96 hours.

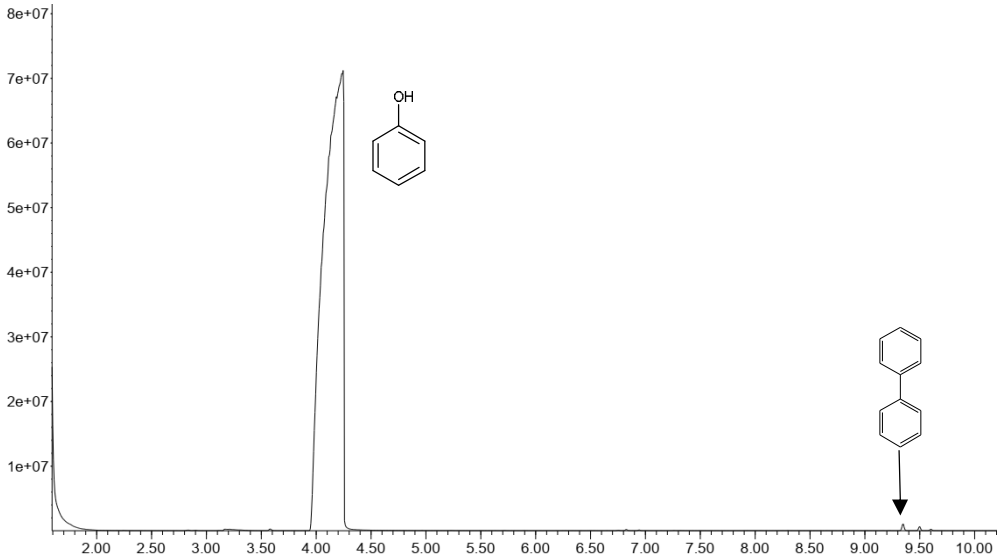

Figure S15. GC-MS profile for the reaction of phenol (5 mmol) catalyzed by **3** (2.5 μmol) in the presence of H_2O_2 (25 mmol) and Et_3N (5.0 μmol) at 60°C.

Scheme S1. The catalytic hydroxylation of cumene with **3**

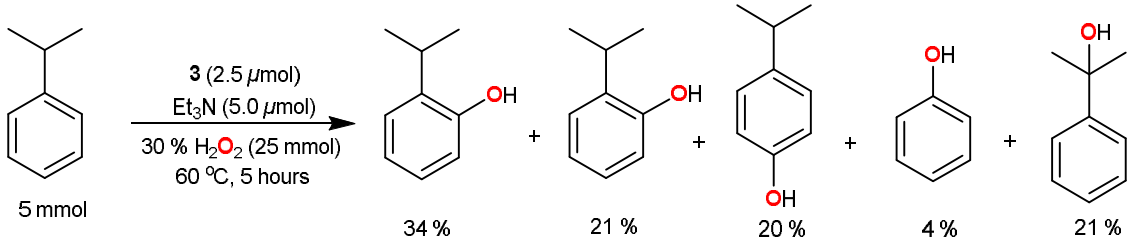

Scheme S2. The catalytic hydroxylation of nitrobenzene with **3**

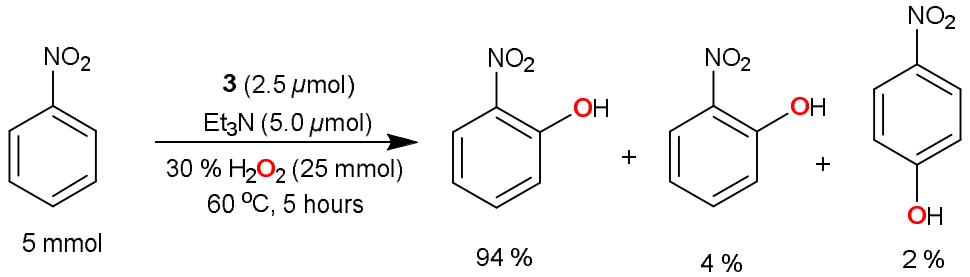

Scheme S3. The catalytic hydroxylation of chlorobenzene with **3**

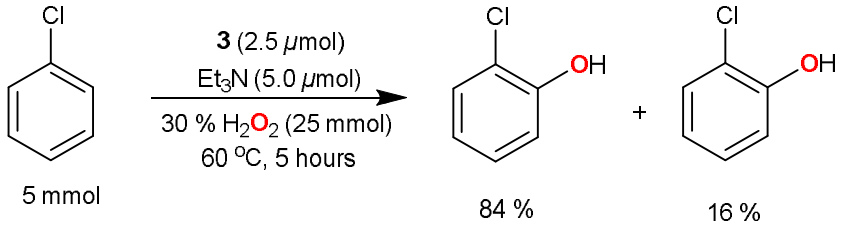

Scheme S4. The catalytic hydroxylation of anisole with **3**

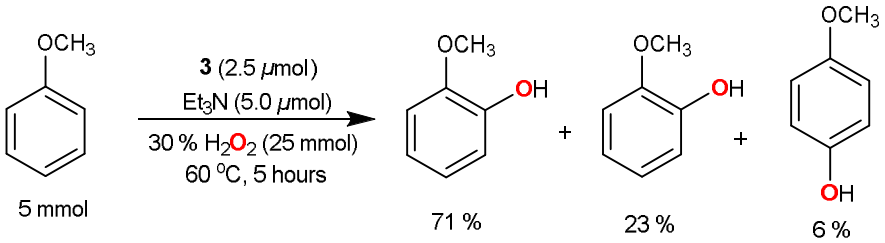

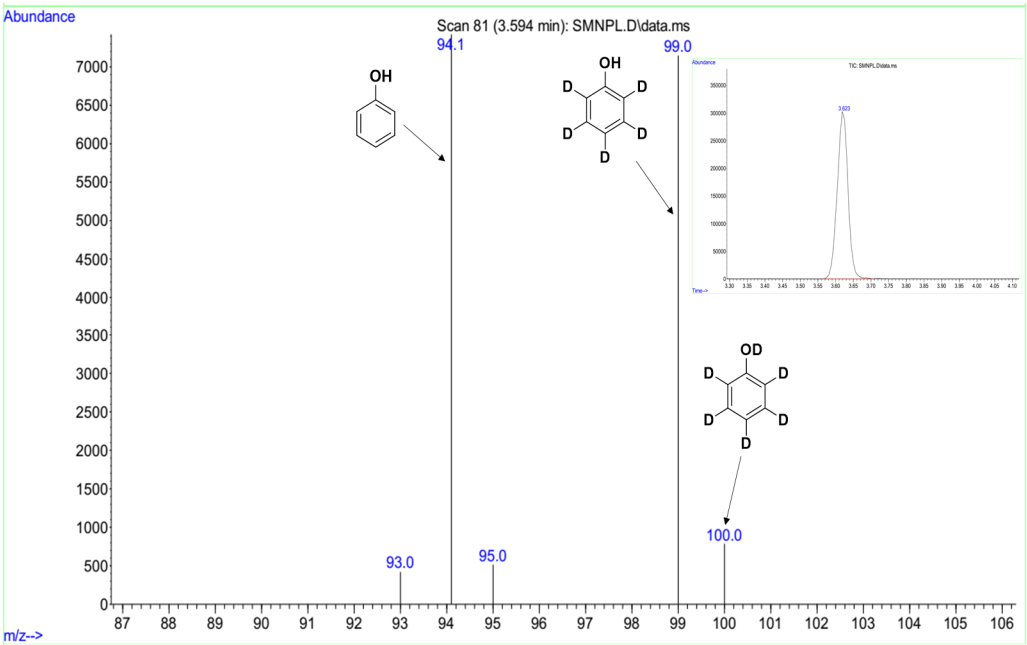

Figure S16. GC-MS profile for the measurement of KIE using C_6H_6 (2.5 mmol) and C_6D_6 (2.5 mmol), **3** (2.5 μmol), H_2O_2 (2.5 mmol) and Et_3N (5 μmol) at 60 °C over 24 hours.

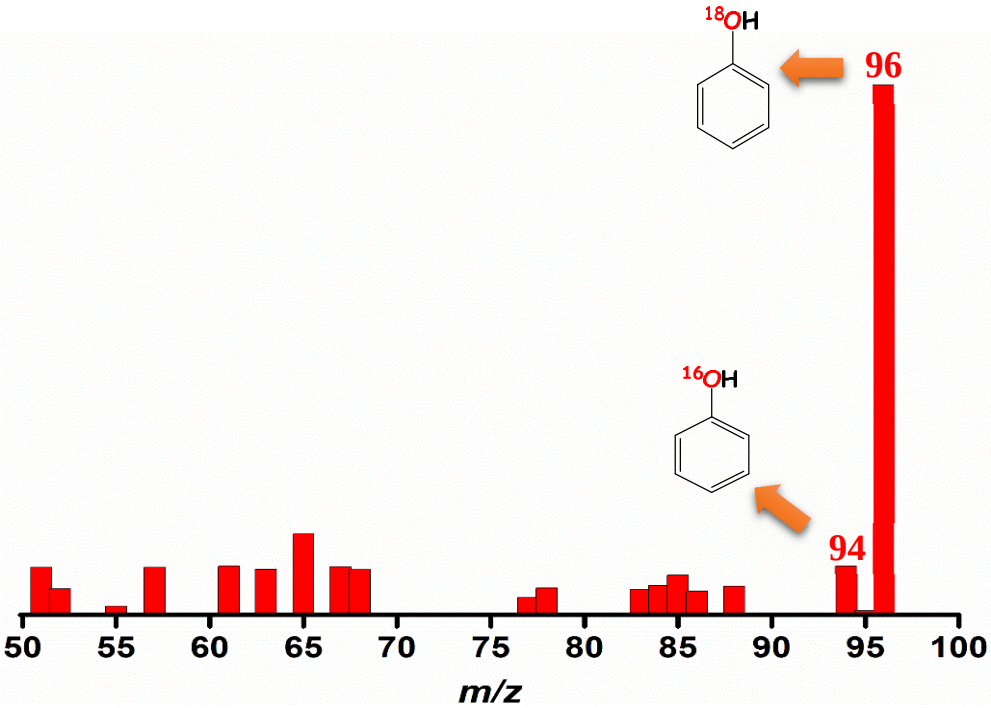

Figure S17. Isotopic labeling studies for the reaction of benzene (0.12 mmol) with $H_2{}^{18}O_2$ (5 equivalents) and Et_3N (5.0 μmol) using catalyst **3**.

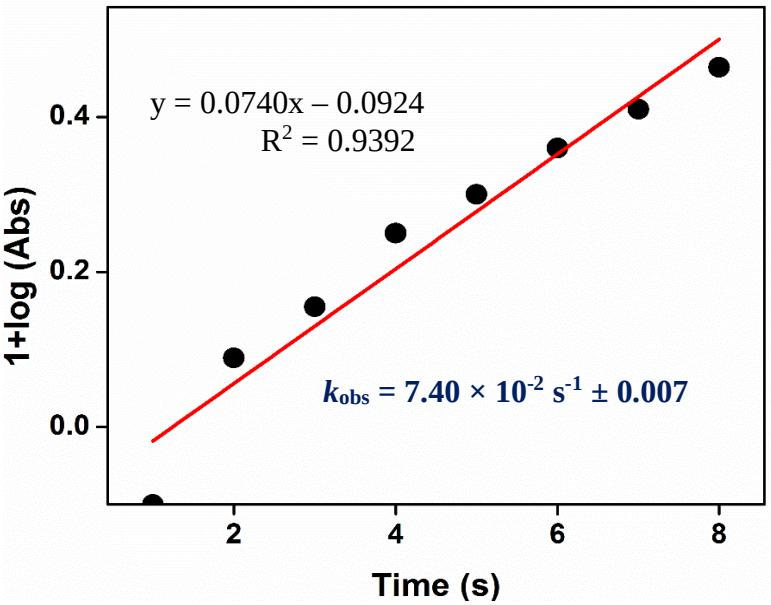

Figure S18. The plot of [1+ log(Abs)] vs time for the calculation of k_{obs} for the formation of $[(L2Ni^{III})_2(\mu\text{-}O)_2]^{2+}$ from **2.**

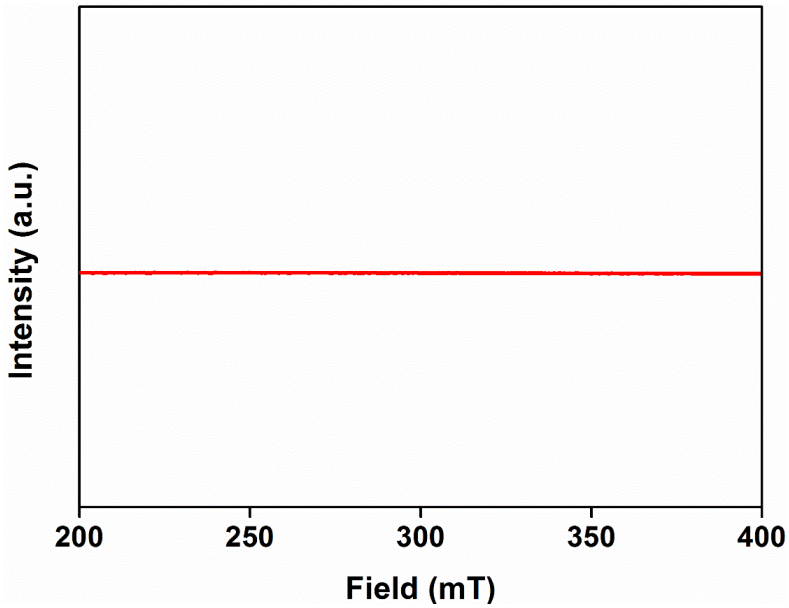

Figure S19. X-band EPR spectrum of $[(L2Ni^{III})_2(\mu\text{-}O)_2]^{2+}$ (1×10^{-4} M), which was generated by addition of H_2O_2 (10 equivalents) to **2** (1×10^{-4} M) in the presence of E_3N (two equivalents) in acetone at -80 °C.

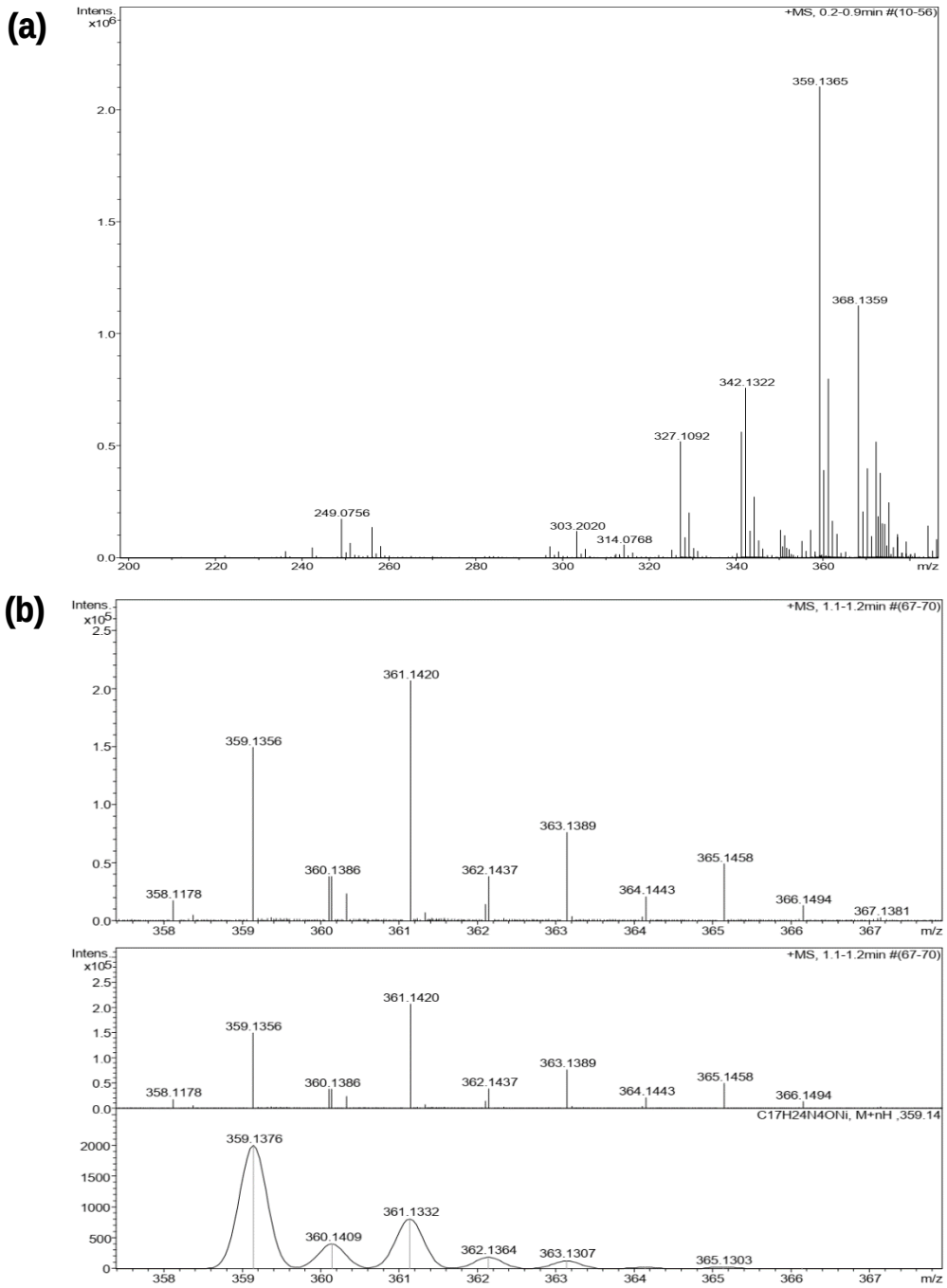

Figure S20. (a) HR-ESI mass spectra for in situ generated $[(L2Ni^{III})_2(\mu\text{-}O)_2]^{2+}$ by reaction of **2** with H_2O_2 (10 equivalents) and E_3N (two equivalents) in acetonitrile. Calculated (*m/z)* for $C_{34}H_{48}N_8Ni_2O_2$ $[M+H]^+$ requires (monoisotopic mass) 359.1304, found 359.1365. **(b)** Experimental (top) and calculated (bottom) HR-ESI mass spectra of $[(L2Ni^{III})_2(\mu\text{-}^{18}O)_2]^{2+}$ by reaction of **2** with $H_2{}^{18}O_2$ (90% ^{18}O atom purity) in acetonitrile. Calculated (*m/z)* for $C_{34}H_{48}N_8Ni_2{}^{18}O_2$ $[M+H]^+$ requires (monoisotopic mass) 361.1424, found 361.1420.

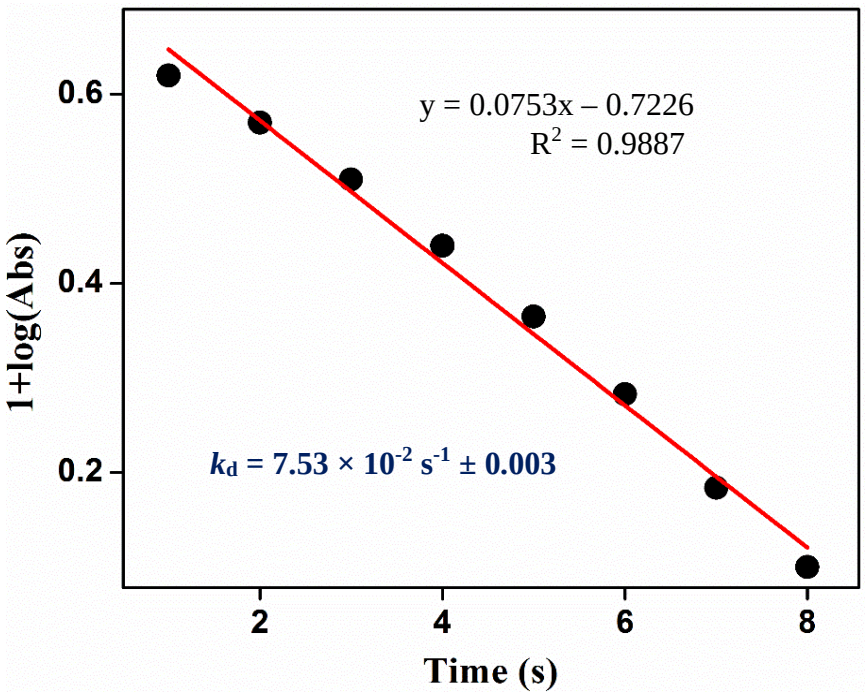

Figure S21. The plot of [1+ log(Abs)] vs time for the decay of $[(L2Ni^{III})_2(\mu\text{-}O)_2]^{2+}$ with benzene.

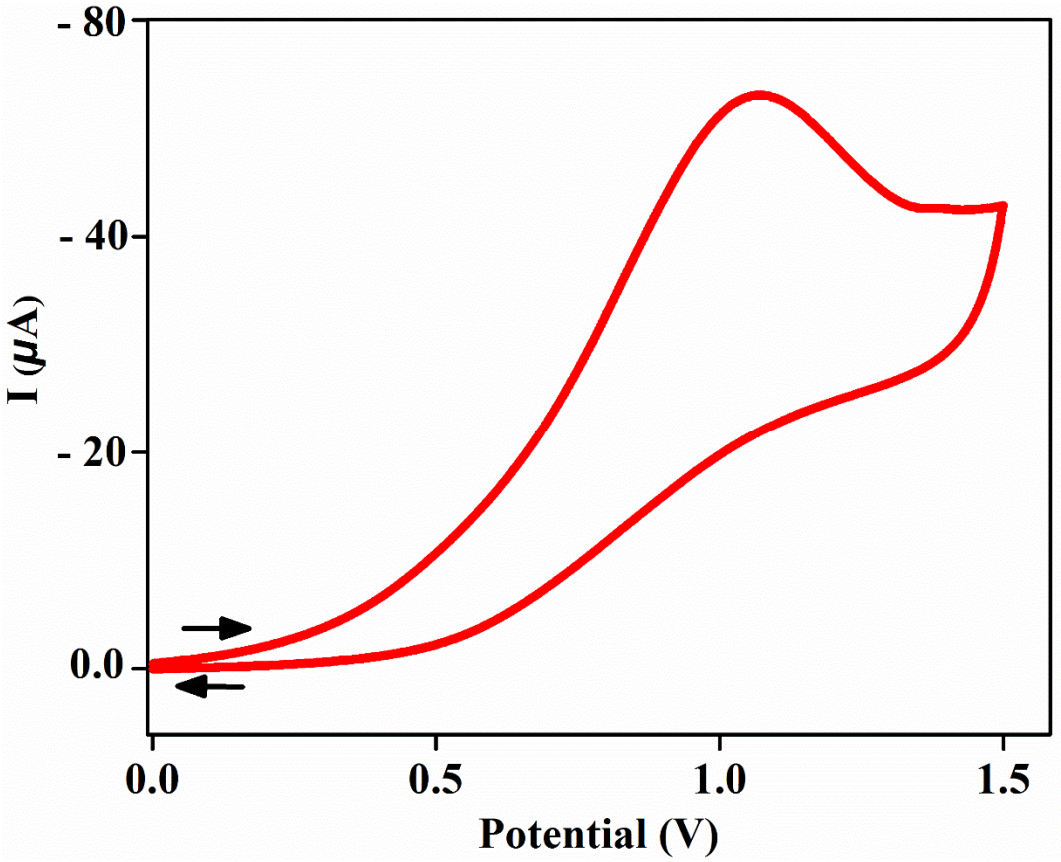

Figure S22. Cyclic voltammogram of **2** (5.0×10^{-3} M) with the addition of 10 equivalents of H_2O_2 and two equivalents of Et_3N in acetonitrile at 25 °C. Supporting electrolyte: 0.5 M TBAP; Reference: Ag/Ag^+; Working electrode: Pt-sphere; Counter electrode: Pt wire; Scan rate = 100 mV s^{-1}.

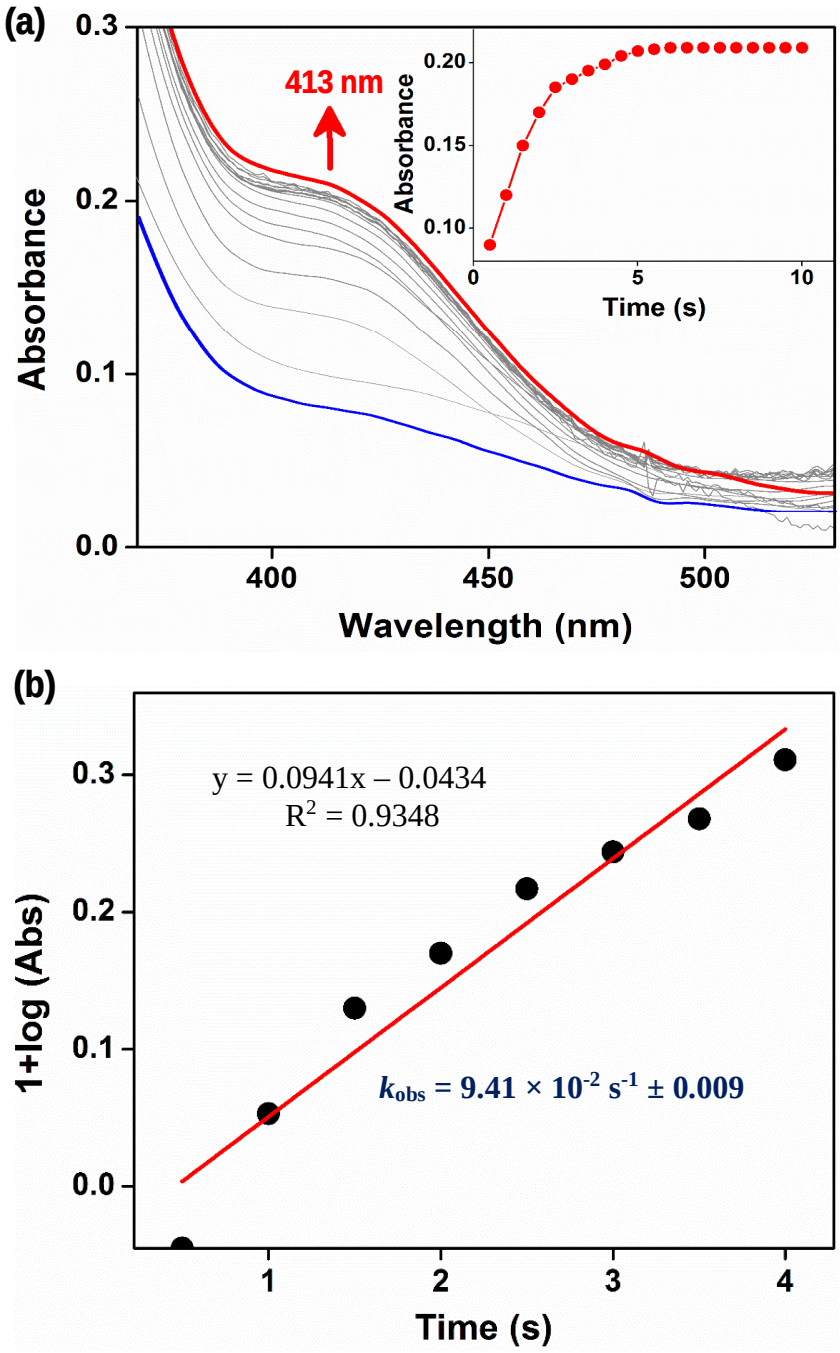

Figure S23. (a) The electronic spectral change observed for **3** (1×10^{-4} M) with 10 equivalents of H_2O_2 and Et_3N (2 equivalents) in CH_3CN: MeOH (8:2) at -40 °C. Spectra were measured in 0.5 second time intervals. Inset: time course of the absorbance at 413 nm. **(b)** The plot of [1+ log(Abs)] vs time for the formation of $[(L3Ni^{III})_2(\mu\text{-}O)_2]^{2+}$.

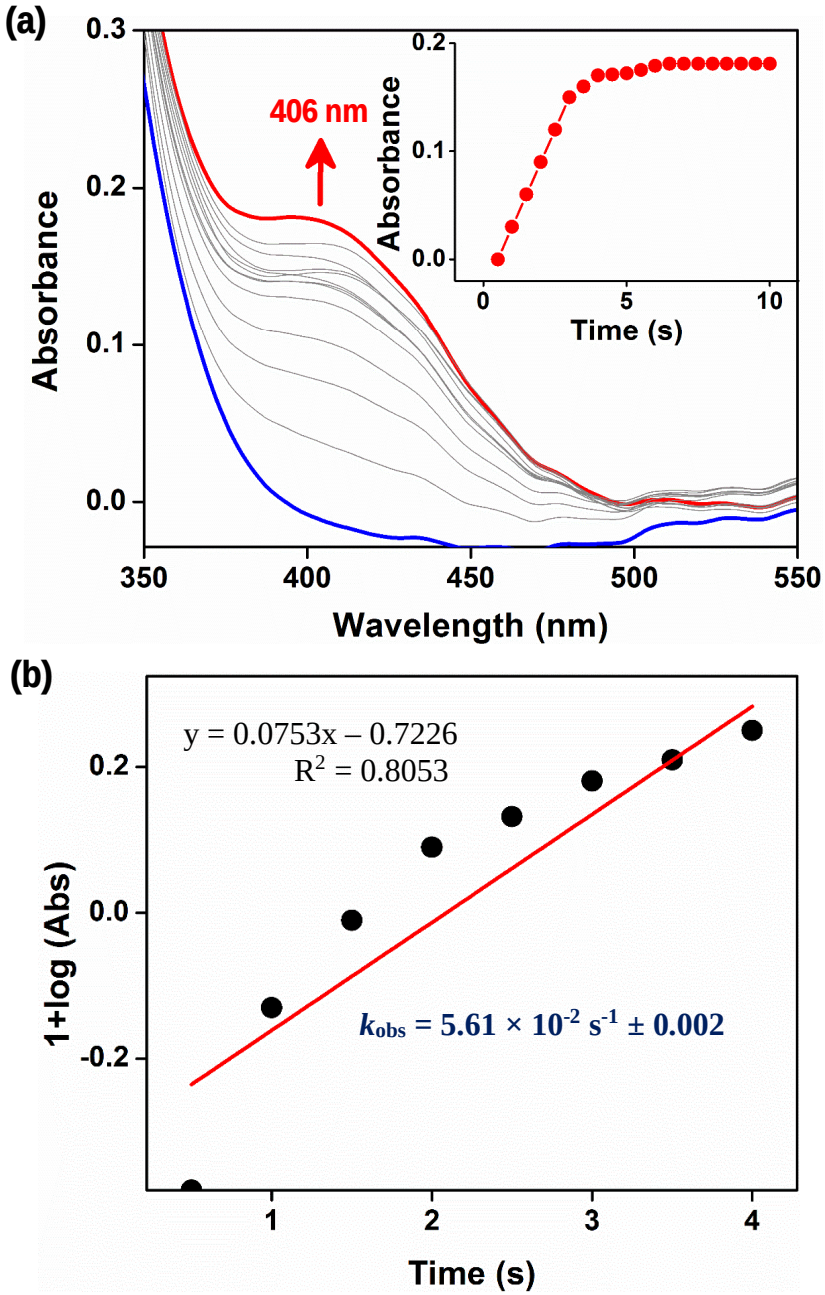

Figure S24. **(a)** The electronic spectral change observed for **4** (1×10^{-4} M) with 10 equivalents of H_2O_2 and Et_3N (2 equivalents) in CH_3CN: MeOH (8:2) at -40 °C. Spectra were measured in 0.5 second time intervals. Inset: time course of the absorbance at 406 nm. **(b)** The plot of [1+ log(Abs)] vs time for the formation of $[(L4Ni^{III})_2(\mu\text{-}O)_2]^{2+}$.

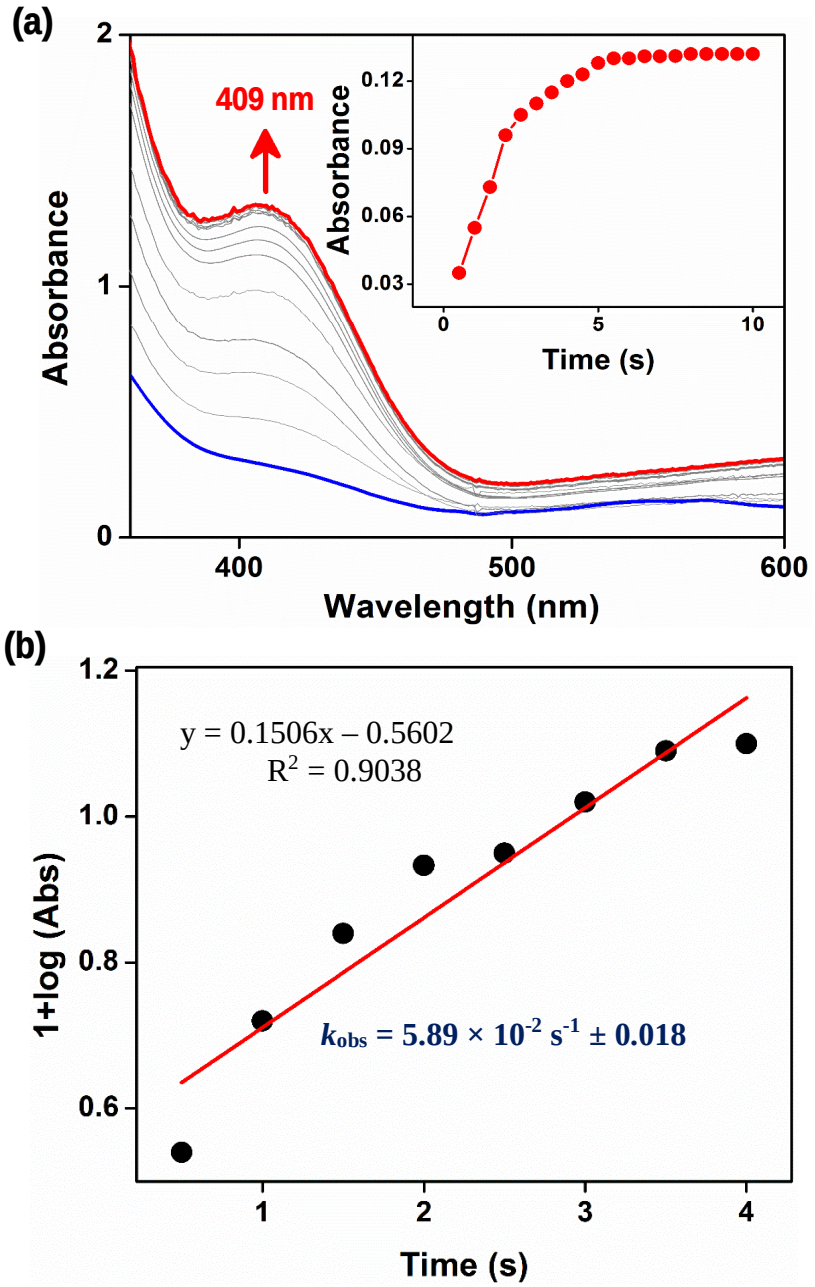

Figure S25. (a) The electronic spectral change observed for **6** (5×10^{-4} M) with 10 equivalents of H_2O_2 and Et_3N (2 equivalents) in CH_3CN: MeOH (8:2) at -40 °C. Spectra were measured in 0.5 second time intervals. Inset: time course of the absorbance at 409 nm. **(b)** The plot of [1+ log(Abs)] vs time for the formation of $[(L6Ni^{III})_2(\mu\text{-}O)_2]^{2+}$.

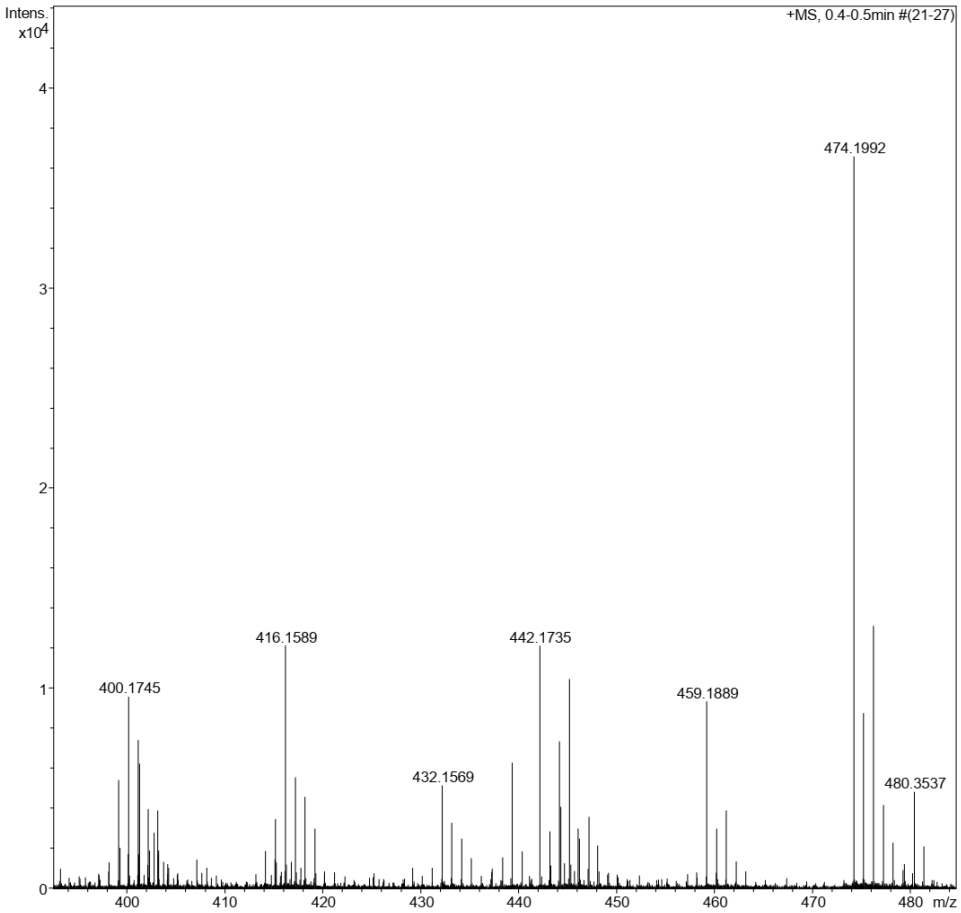

Figure S26. HR-ESI mass spectra for in situ generated $[(L3Ni^{III})_2(\mu\text{-}O)_2]^{2+}$ from **3** with H_2O_2 (10 equivalents) and E_3N (2 equivalents) in acetonitrile. Calculated value (*m/z)* for $C_{46}H_{72}N_8Ni_2O_6$ $[M]^+$ (monoisotopic mass), 474.2141 and found value, 474.1992.

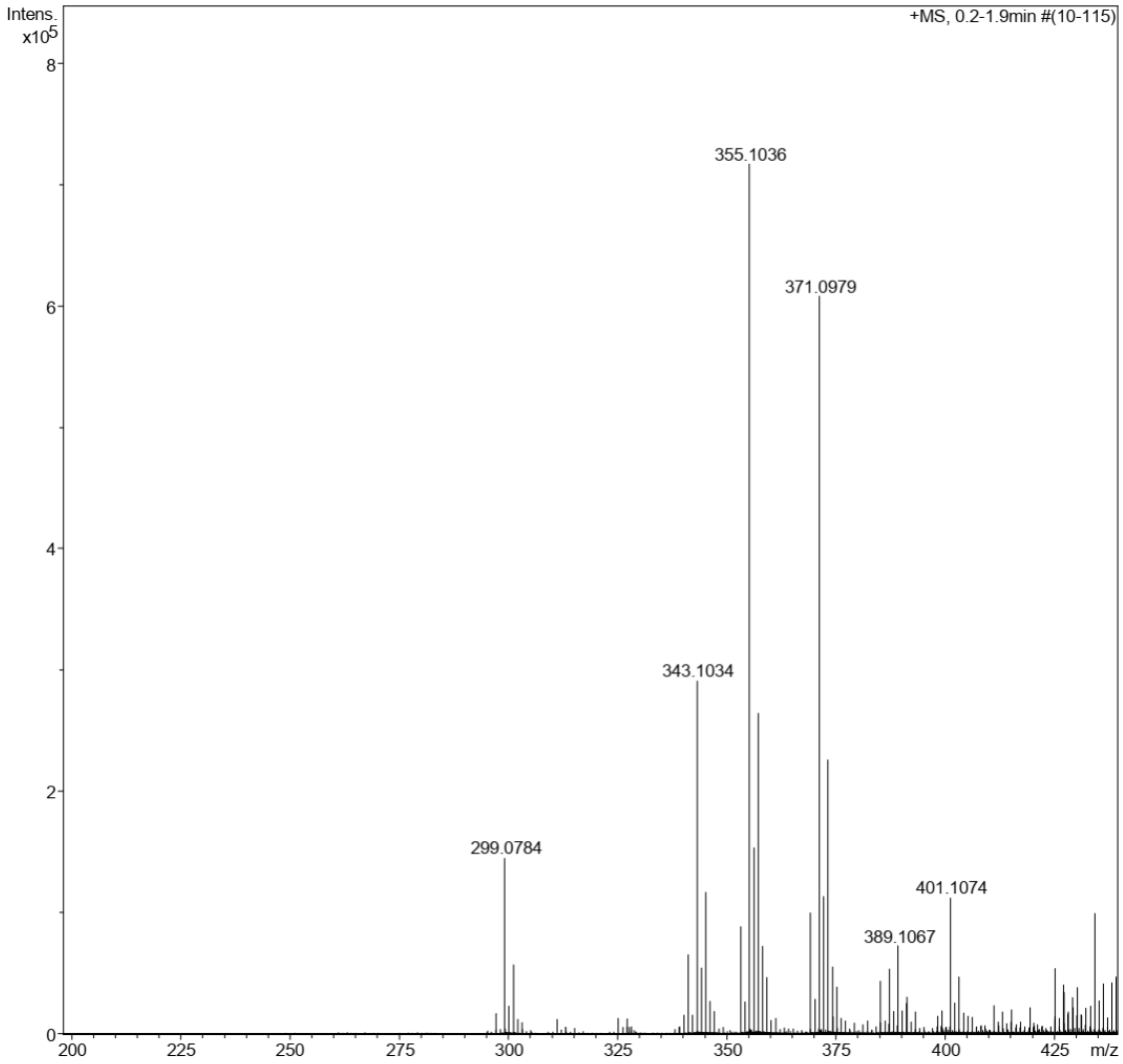

Figure S27. HR-ESI mass spectra for in situ generated $[(L4Ni^{III})_2(\mu\text{-}O)_2]^{2+}$ from **4** with H_2O_2 (10 equivalents) and E_3N (2 equivalents) in acetonitrile. Calculated (*m/z)* value for $C_{34}H_{44}N_8Ni_2O_2$ $[M\text{-}H]^+$ (monoisotopic mass), 355.1069 and found value, 355.1036.

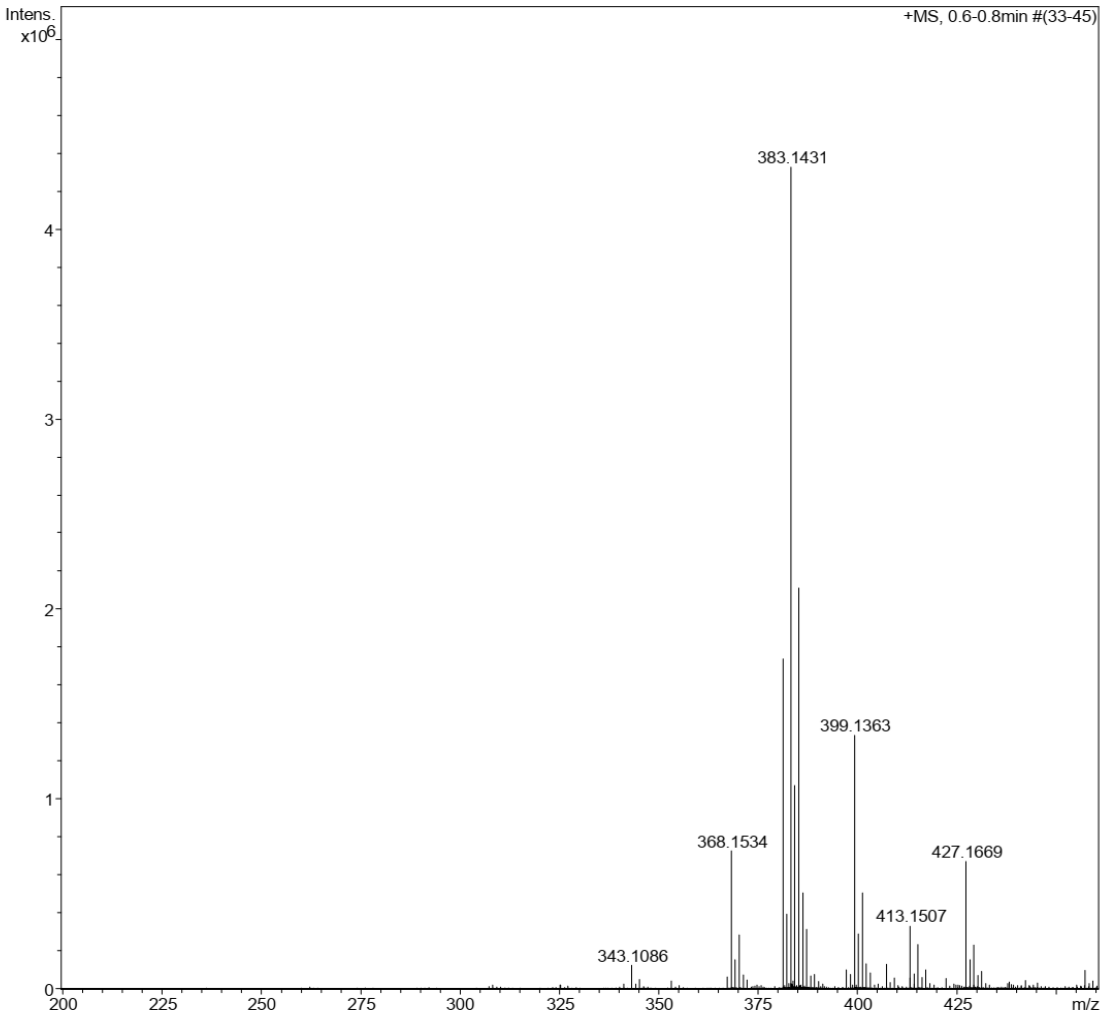

Figure S28. HR-ESI mass spectra for in situ generated $[(L6Ni^{III})_2(\mu\text{-}O)_2]^{2+}$ from **6** with H_2O_2 (10 equivalents) and E_3N (2 equivalents) in acetonitrile. Calculated value (*m/z)* for $C_{38}H_{52}N_8Ni_2O_2$ $[M\text{-}H]^+$ (monoisotopic mass), 383.1382 and found value, 383.1431.

	HOMO	LUMO +1	Energy gap (eV)
$[(L2Ni^{III})_2(\mu\text{-}O)_2]^{2+}$	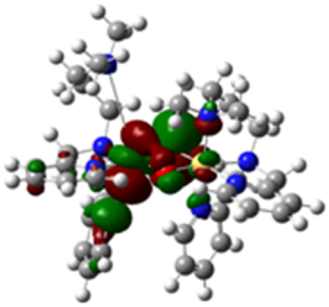	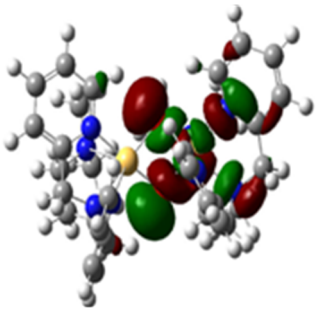	**2.8398**
$[Ni^{III}(L2)(OOH)]^{2+}$	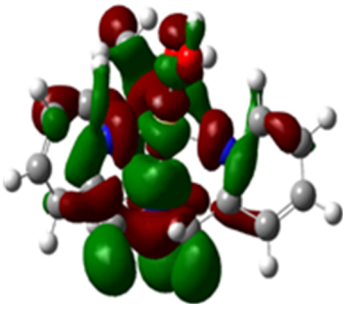	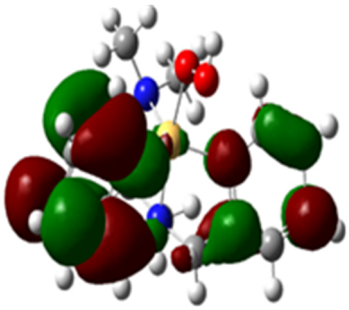	**5.7113**
$[Ni^{III}(O_2)(L2)]^{+}$	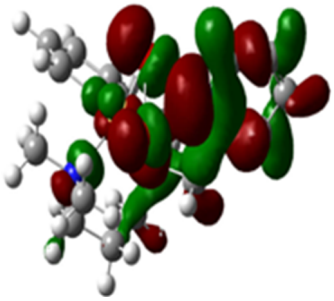	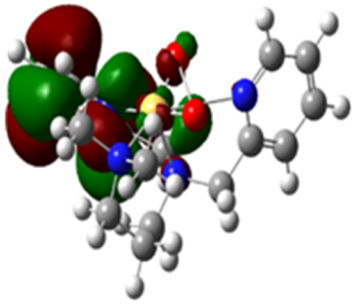	**4.6613**

Figure S29. DFT of optimized HOMO and LUMO+1 of intermediates

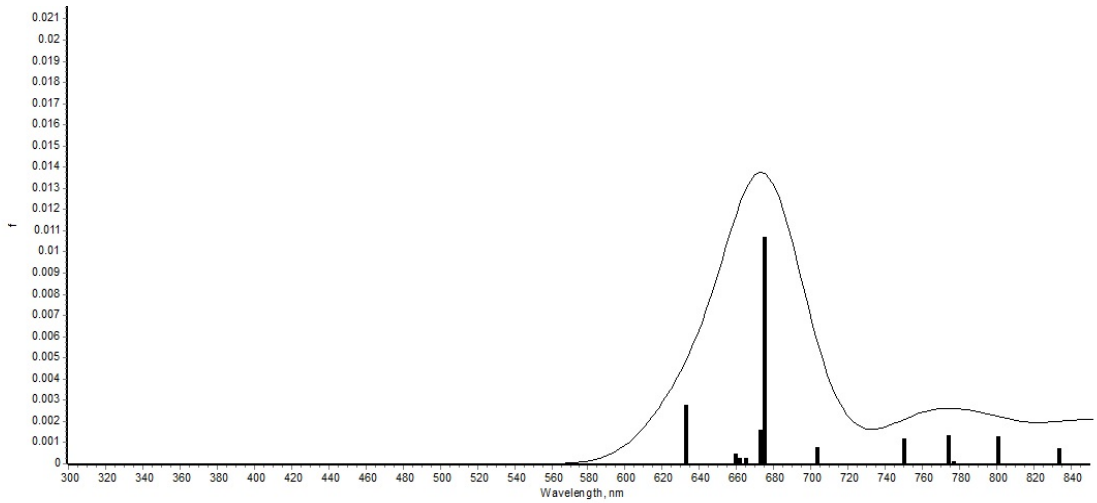

Figure S30. Calculated electronic spectra of $[(L2Ni^{III})_2(\mu\text{-}O)_2]^{2+}$ by TD-DFT method.

Table S1 Selected bond distance[a] (Å) bond angle(°) for complex **2**.

2			
Ni(1)-N(1)	2.105(3)	N(5)-Ni(1)-N(1)	93.20(12)
Ni(1)-N(2)	2.132(3)	N(5)-Ni(1)-N(3)	91.20(12)
Ni(1)-N(3)	2.109(3)	N(1)-Ni(1)-N(3)	83.23(11)
Ni(1)-N(4)	2.151(3)	N(5)-Ni(1)-N(6)	91.83(13)
Ni(1)-N(5)	2.101(3)	N(1)-Ni(1)-N(6)	85.66(13)
Ni(1)-N(6)	2.126(3)	N(3)-Ni(1)-N(6)	168.63(13)
		N(5)-Ni(1)-N(2)	171.40(12)
		N(1)-Ni(1)-N(2)	80.53(12)
		N(3)-Ni(1)-N(2)	82.26(12)
		N(6)-Ni(1)-N(2)	93.54(13)
		N(5)-Ni(1)-N(4)	90.78(12)
		N(1)-Ni(1)-N(4)	174.55(13)
		N(3)-Ni(1)-N(4)	100.43(12)
		N(4)-Ni(1)-N(6)	90.49(13)
		N(2)-Ni(1)-N(4)	95.88(12)

[a]Standard deviations in parenthesis

Table S2. Crystal Data and Structure Refinement for complexes **2.**

	2
Formula	$C_{69}H_{70}B_2N_6Ni$
FW	1063.64
Cryst. system	Orthorhombic
Space group	P_{bca}
Temperature	293 k
a/Å	35.8282(17)
b/Å	18.7973(8)
c/A^0	17.4964(7)
$\alpha/^0$	90
$\beta/^0$	90
$\gamma/^0$	90
Volume/$Å^3$	11783.4(9)
Z	8
ρ_{calc}mg/mm^3	1.199
μ/mm^{-1}	0.376
F(000)	4512
Reflection collected	41779
Goodness-of-fit on F^2	1.074
$R1^a$	0.0762
$wR2^b$	0.1700

$^aR1=\sum ||F_o|-|Fc||/\sum|F_o|$, $^bWR_2=\sum w[(F_o-F_c)^2/\sum w[(F_o^2)^2]^{1/2}$

Table S3. Electronic Spectral and Redox data for **1 - 6**.

Complexes	λ_{max}, nm (ε, M^{-1} cm^{-1})[a]	Redox data[b]	
		CV E_{ox} (V)	DPV (V)
1	554 (73), 790 (48), 903 (82)	1.008	0.912
2	545 (99), 788 (91), 855 (101)	1.024	0.926
3	362 (76, sh), 561 (30), 783 (10), 918 (22)	1.051	0.940
4	468 (64), 787 (47), 843 (46)	0.990	0.863
5	594 (63), 792 (24), 898 (23)	0.966	0.851
6	375 (88, sh), 481 (28), 782 (19), 852 (25)	0.997	0.876

[a]Concentration: 5×10^{-3} M in CH_3CN at 25 ºC. [b]Concentration: 5×10^{-3} M in CH_3CN at 25 ºC. Supporting electrolyte: 0.5 M TBAP; Reference: Ag/Ag^+; Working electrode: Pt-sphere; Counter electrode: Pt wire; Scan rate = 100 mV s^{-1}.

Table S4: Influence of [H_2O_2] concentration for benzene hydroxylation catalyzed by **3.**

Entry[a]	[H_2O_2] (mmol)	Conversion (%)	Yield (%)	Selectivity (%)
1	5	31	30	>99
2	10	34	33	98
3	15	37	35	97
4	20	39	38	97
5	25	42	41	97
6	30	48	41	86
7	35	53	42	79
8	40	59	43	72
9	45	64	43	67
10	50	65	43	67

[a]Reaction condition: benzene (5 mmol), catalyst **3** (2.5 μmol, 0.05%) and triethylamine (5.0 μmol), hydrogen peroxide (30%) (5 mmol to 50 mmol) in acetonitrile at 60 °C for 5 hours.

Table S5: Catalytic hydroxylation of benzene with equal amount of H_2O_2 using **1 – 6**.

Complex	Temperature (°C)	Conversion (%)	Selectivity (%)	Yield[a] (%)	TON	TOF(h^{-1})
1	60°C	39	65	25	500	100
	25°C	16	78	12	240	48
2	60°C	31	87	27	540	108
	25°C	16	89	14	280	56
3	60°C	31	99	30	600	120
	25°C	15	99	15	300	60
4	60°C	25	62	15	300	60
	25°C	16	71	12	240	48
5	60°C	20	57	12	240	48
	25°C	10	73	7	140	28
6	60°C	27	66	18	360	72
	25°C	18	77	14	280	56

[a]Reaction condition: benzene (5 mmol), catalyst (2.5 μmol, 0.05%) and triethylamine (5.0 μmol), hydrogen peroxide (30%) (5 mmol) in acetonitrile for 5 hours.

Table S6. Calculated bond distance and bond angle for $[(L2Ni^{III})_2(\mu\text{-}O)_2]^{2+}$ by TD-DFT method.

$[(L2Ni^{III})_2(\mu\text{-}O)_2]^{2+}$			
Ni(1)-N(1)	1.66	N(4)-Ni(1)-N(3)	79.98
Ni(1)-N(2)	2.15	N(4)-Ni(1)-N(1)	72.98
Ni(1)-N(3)	2.04	N(4)-Ni(1)-N(1)	138.24
Ni(1)-N(4)	2.09	N(3)-Ni(1)-N(1)	82.85
Ni(1)-O(1)	1.80	N(3)-Ni(1)-N(2)	85.90
Ni(1a)-O(2)	1.84	N(1)-Ni(1)-N(2)	68.04
		O(1)-Ni(1)-O(2)	81.34
		O(1)-Ni(1a)-O(2)	83.60
		O(2)-Ni(1)-N(1)	101.61
		O(2)-Ni(1)-N(2)	95.44
		O(2)-Ni(1)-N(3)	175.52
		O(2)-Ni(1)-N(4)	96.30

Table S7a. Coordinates for the optimized geometry of $[(L2Ni^{III})_2(\mu\text{-}O)_2]^{2+}$

Standard Orientation:

Center Number	Atomic Number	Atomic Type	Coordinates (Angstroms) X	Y	Z
1	6	0	5.045962	1.018302	2.603673
2	6	0	3.894445	0.611948	3.282351
3	6	0	2.790842	0.163775	2.552884
4	7	0	2.855853	0.109394	1.190661
5	6	0	3.963484	0.516124	0.509483
6	6	0	5.084280	0.977514	1.208203
7	6	0	3.947516	0.439104	-1.003455
8	7	0	2.667523	-0.188774	-1.491072
9	6	0	1.938423	0.740204	-2.412382
10	6	0	1.455787	1.838207	-1.567365
11	7	0	1.181253	1.465571	-0.294956
12	6	0	1.241256	2.418996	0.692649
13	6	0	1.353876	3.780440	0.371696
14	6	0	1.485569	4.162096	-0.962514
15	6	0	1.580843	3.180252	-1.942720
16	6	0	2.897200	-1.412668	-2.281250
17	6	0	3.651465	-2.494728	-1.541934
18	6	0	3.293659	-2.561164	-0.054000
19	7	0	1.842904	-2.329835	0.331203
20	6	0	1.935399	-2.674147	1.804525
21	6	0	1.182519	-3.417186	-0.446861
22	28	0	1.493890	-0.341405	0.024714
23	6	0	-1.909477	4.110990	-0.778145
24	6	0	-1.590934	3.678390	0.506675
25	6	0	-1.337567	2.317909	0.729326
26	7	0	-1.336401	1.416656	-0.306896
27	6	0	-1.768493	1.827254	-1.509843
28	6	0	-2.034204	3.171982	-1.798207
29	6	0	-2.133166	0.723056	-2.369394
30	7	0	-2.738203	-0.309479	-1.471998
31	6	0	-4.040593	0.211271	-0.904049
32	6	0	-3.987245	0.277808	0.612199
33	7	0	-2.823074	-0.042667	1.241460
34	6	0	-2.698691	-0.018541	2.599422
35	6	0	-3.798246	0.334326	3.384987
36	6	0	-5.005587	0.667528	2.763853
37	6	0	-5.105790	0.643233	1.369787
38	6	0	-2.995209	-1.479217	-2.386355
39	6	0	-1.845250	-2.455576	-2.435075
40	6	0	-1.785631	-3.230353	-1.124342
41	7	0	-1.873945	-2.396717	0.140695
42	6	0	-3.325436	-2.623377	0.553140
43	6	0	-1.279084	-3.018227	1.322745
44	28	0	-1.483320	-0.415893	0.041482

45	8	0	0.016771	-0.821825	-1.057422
46	8	0	0.015434	-0.415082	1.284554
47	1	0	5.904668	1.372816	3.158811
48	1	0	3.852769	0.656968	4.362800
49	1	0	1.889317	-0.115351	3.076609
50	1	0	5.972948	1.297402	0.678975
51	1	0	4.090106	1.471879	-1.392841
52	1	0	4.839963	-0.125894	-1.343294
53	1	0	1.058710	0.256876	-2.879477
54	1	0	2.585001	1.099883	-3.246135
55	1	0	1.201077	2.132141	1.733029
56	1	0	1.359937	4.528062	1.153671
57	1	0	1.597336	5.206256	-1.224188
58	1	0	1.822464	3.456133	-2.961716
59	1	0	1.919000	-1.811549	-2.601312
60	1	0	3.444672	-1.202738	-3.229107
61	1	0	4.752054	-2.349033	-1.602819
62	1	0	3.454009	-3.448541	-2.076945
63	1	0	3.685247	-3.549754	0.299142
64	1	0	3.965689	-1.874321	0.469031
65	1	0	1.210474	-2.154642	2.452011
66	1	0	2.886941	-2.369526	2.294625
67	1	0	1.874838	-3.771491	1.984469
68	1	0	0.574304	-4.102348	0.155576
69	1	0	0.778628	-3.050856	-1.393219
70	1	0	1.848496	-4.254311	-0.761722
71	1	0	-2.125822	5.154840	-0.963523
72	1	0	-1.559877	4.381371	1.329178
73	1	0	-1.158688	1.984909	1.741730
74	1	0	-2.388800	3.476578	-2.774332
75	1	0	-2.812751	1.054999	-3.188957
76	1	0	-1.206108	0.338494	-2.833910
77	1	0	-4.907676	-0.424522	-1.183502
78	1	0	-4.304458	1.223711	-1.284220
79	1	0	-1.758409	-0.263880	3.071566
80	1	0	-3.714436	0.355407	4.463765
81	1	0	-5.863144	0.944771	3.363055
82	1	0	-6.040935	0.898490	0.887702
83	1	0	-3.214271	-1.142968	-3.427851
84	1	0	-3.911887	-2.054629	-2.159281
85	1	0	-0.909175	-1.962978	-2.735918
86	1	0	-2.031593	-3.195539	-3.245728
87	1	0	-2.634427	-3.951792	-1.216246
88	1	0	-1.030531	-4.010256	-1.144841
89	1	0	-3.613264	-2.227575	1.547964
90	1	0	-4.076679	-2.246825	-0.135915
91	1	0	-3.580656	-3.707164	0.667892
92	1	0	-1.628710	-2.596730	2.293048
93	1	0	-0.314625	-2.719988	1.339652
94	1	0	-1.378226	-4.129370	1.340216

Table S7b. Coordinates for the optimized geometry of $[Ni^{III}(O_2)(L2)]^+$:

Standard Orientation:

Center Number	Atomic Number	Atomic Type	Coordinates (Angstroms) X	Y	Z
1	6	0	4.367224	-1.598674	-0.367090
2	6	0	3.735784	-1.363536	-1.608647
3	6	0	2.433011	-0.851670	-1.688947
4	7	0	1.769325	-0.590800	-0.540813
5	6	0	2.452904	-0.828844	0.840986
6	6	0	3.739817	-1.332388	0.860735
7	6	0	1.405529	-0.347257	2.291375
8	7	0	-0.160965	0.264236	1.758738
9	6	0	-1.368500	-0.639074	2.110495
10	6	0	-2.147107	-1.057316	0.809277
11	7	0	-1.619328	-0.742138	-0.440571
12	6	0	-2.256262	-1.096420	-1.592847
13	6	0	-3.467339	-1.789994	-1.529342
14	6	0	-4.012520	-2.121230	-0.286022
15	6	0	-3.350893	-1.761960	0.890113
16	6	0	-0.483303	1.661596	2.243006
17	6	0	-0.139222	2.828964	1.275251
18	6	0	-0.898591	2.771282	-0.087744
19	7	0	-0.367472	1.788704	-1.087276
20	6	0	0.889479	2.323629	-1.685436
21	6	0	-1.337575	1.703787	-2.197261
22	28	0	-0.013774	0.139071	-0.177909
23	8	0	0.281506	-0.806708	0.419027
24	8	0	0.876369	0.656323	0.360138
25	1	0	5.375512	-1.992153	-0.361493
26	1	0	4.272302	-1.582359	-2.522803
27	1	0	1.963448	-0.676637	-2.647181
28	1	0	4.249933	-1.509346	1.798212
29	1	0	1.267927	-1.223172	2.958741
30	1	0	1.942904	0.441694	2.858462
31	1	0	-2.066410	-0.177628	2.842049
32	1	0	-1.020649	-1.574107	2.598220
33	1	0	-1.830348	-0.885569	-2.558254
34	1	0	-3.975351	-2.081120	-2.439694
35	1	0	-4.947297	-2.664211	-0.234431
36	1	0	-3.772882	-2.023674	1.852164
37	1	0	-1.577338	1.799505	2.391028
38	1	0	-0.014042	1.827299	3.236072
39	1	0	0.954109	2.956350	1.141141
40	1	0	-0.486802	3.749022	1.795357
41	1	0	-1.966674	2.560783	0.145553
42	1	0	-0.874360	3.792587	-0.533995

43	1	0	1.685190	2.485341	-0.931199
44	1	0	1.290456	1.615868	-2.439426
45	1	0	0.723375	3.301599	-2.191629
46	1	0	-0.966463	1.025587	-2.992585
47	1	0	-2.340628	1.399448	-1.838363
48	1	0	-1.488781	2.698607	-2.675760

Table S7c. Coordinates for the optimized geometry of $[Ni^{III}(L2)(OOH)]^{2+}$

Standard Orientation:

Center Number	Atomic Number	Atomic Type	Coordinates (Angstroms) X	Y	Z
1	6	0	4.406962	-0.122367	-1.802271
2	6	0	4.001328	1.181355	-1.452436
3	6	0	2.763534	1.355509	-0.823852
4	7	0	1.942218	0.302834	-0.529686
5	6	0	2.340288	-0.967055	-0.850515
6	6	0	3.564001	-1.205609	-1.497035
7	6	0	1.445623	-2.117101	-0.410378
8	7	0	0.041719	-1.667092	-0.119262
9	6	0	-0.853542	-1.835057	-1.326148
10	6	0	-2.094357	-0.964719	-1.198363
11	7	0	-1.940691	0.199761	-0.493219
12	6	0	-2.998820	1.047055	-0.359179
13	6	0	-4.247504	0.770218	-0.931013
14	6	0	-4.409014	-0.421808	-1.663597
15	6	0	-3.317427	-1.301934	-1.793777
16	6	0	-0.565897	-2.363775	1.077631
17	6	0	0.152786	-2.118150	2.427560
18	6	0	0.860993	-0.762886	2.647506
19	7	0	0.108580	0.477374	2.206694
20	6	0	0.925518	1.683681	2.609232
21	6	0	-1.240346	0.565229	2.869815
22	28	0	0.003401	0.410001	0.133647
23	8	0	0.022131	2.655044	-0.149862
24	8	0	-0.793797	3.156259	-1.141367
25	1	0	5.357588	-0.289685	-2.299431
26	1	0	4.626523	2.041738	-1.664884
27	1	0	2.412771	2.342087	-0.543864
28	1	0	3.855620	-2.220347	-1.751043
29	1	0	1.451292	-2.914201	-1.165205
30	1	0	1.867850	-2.555259	0.500517
31	1	0	-1.134608	-2.888996	-1.455041
32	1	0	-0.283215	-1.538877	-2.217068
33	1	0	-2.834823	1.953277	0.211481
34	1	0	-5.067950	1.467871	-0.803506
35	1	0	-5.365158	-0.663937	-2.117528
36	1	0	-3.418776	-2.230892	-2.346342

37	1	0	-1.601734	-2.017982	1.137082
38	1	0	-0.602647	-3.446485	0.885341
39	1	0	0.917272	-2.887679	2.594958
40	1	0	-0.593567	-2.283210	3.213878
41	1	0	1.083842	-0.670931	3.721190
42	1	0	1.822190	-0.739189	2.123369
43	1	0	1.915717	1.633656	2.148059
44	1	0	0.422224	2.599861	2.289898
45	1	0	1.048731	1.715149	3.700122
46	1	0	-1.720965	1.508305	2.594628
47	1	0	-1.880128	-0.260963	2.555792
48	1	0	-1.133195	0.537665	3.962941
49	1	0	-0.534289	4.112918	-1.278402

Table S8. Excitation energy and Oscillator strength

State	Energy (cm^{-1})	Wavelength (nm)	fosc
1	11998.1	833.5	0.000729146
2	12490.0	800.6	0.001259139
3	12873.3	776.8	0.000102903
4	13331.0	750.1	0.001201729
5	15046.8	664.6	0.000249906
6	15123.7	661.2	0.000235045
7	11757.1	850.6	0.001175879
8	12926.6	773.6	0.001309037
9	15163.6	659.5	0.000475987
10	14219.7	703.3	0.000761313
11	14867.2	672.6	0.001581364
12	15813.8	632.4	0.002786700
13	14817.4	674.9	0.010707375

Table S9. Calculated energy for optimized structures:

	Energy (ev)
$[(L2Ni^{III})_2(\mu\text{-}O)_2]^{2+}$	-61252.83
$[Ni^{III}(L2)(OOH)]^{2+}$	-32680.87
$[Ni^{III}(O_2)(L2)]^{+}$	-32653.66

Reply for Check CIF alerts for complex 2:

Alert Level B:

PLAT910_ALERT_3_B Missing # of FCF Reflection(s) Below Theta(Min) 13 Note

Authors Response: The unit cell is reasonable large and these low angle reflections are probably missing due to the beam stop.

Alert Level C:

PLAT052_ALERT_1_C Info on Absorption Correction Method Not Given Please Do !
PLAT341_ALERT_3_C Low Bond Precision on C-C Bonds ..... 0.00635 Ang.
PLAT906_ALERT_3_C Large K Value in the Analysis of Variance ..... 11.954 Check
PLAT906_ALERT_3_C Large K Value in the Analysis of Variance ..... 2.990 Check
PLAT911_ALERT_3_C Missing FCF Refl Between Thmin & STh/L= 0.600 3 Report
PLAT934_ALERT_3_C Number of (Iobs-Icalc)/SigmaW > 10 Outliers .... 1 Check
PLAT978_ALERT_2_C Number C-C Bonds with Positive Residual Density. 0 Info

Authors Response: RIGU restraints were applied to atoms in the disordered chains. Several of the atoms were still not ideally shaped, however, this does not indicate an incorrect atom-type assignment.

Alert Level G:

PLAT083_ALERT_2_G SHELXL Second Parameter in WGHT Unusually Large 23.40 Why ?
PLAT199_ALERT_1_G Reported _cell_measurement_temperature ..... (K) 293 Check
PLAT200_ALERT_1_G Reported _diffrn_ambient_temperature ..... (K) 293 Check
PLAT794_ALERT_5_G Tentative Bond Valency for Ni1 (II) . 1.93 Info
PLAT912_ALERT_4_G Missing # of FCF Reflections Above STh/L= 0.600 1496 Note
PLAT950_ALERT_5_G Calculated (ThMax) and CIF-Reported Hmax Differ 2 Units
PLAT956_ALERT_1_G Calculated (ThMax) and Actual (FCF) Hmax Differ 2 Units

Authors Response: Crystals diffracted extremely weakly. Multiple attempts were made to grow better diffracting crystals. Data was collected at three different facilities with radiation sources of Mo, Cu and synchrotron. All results were consistent with the model in this report (from the Cu data collection), however, all yielded serious problems due to weak diffraction and disorder in the atom positions.